

Investigating magnetic hysteresis with op-amp integrator circuit[†]

T. K. Lam^a

Experiment: 22 November 2022 | Submitted: 08 December 2022 | Word count: 2900*

ABSTRACT Magnetic hysteresis in several ferromagnetic materials (mild steel, transformer core iron, Cu/Ni alloy) was studied by constructing a system consisting of two solenoid coils and an op-amp integrator circuit. Hysteresis loops were constructed by measuring the magnetic flux density (B -field) response of the materials to externally applied magnetic fields (H -field), allowing us to correctly identify mild steel as the most ferromagnetic material with the greatest magnetic power dissipation ($12.4 \pm 1.3 \text{ mWm}^{-3}$). Monte Carlo error propagation was performed to show that the greatest source of experimental error came from measuring material dimensions. The experimental data was also found to fit the original Jiles–Atherton model poorly. Finally, heat-induced ferromagnetic to paramagnetic change observed in the Cu/Ni alloy by making measurements at 5°C and 54°C suggests the system constructed could be modified to quantify the Curie temperature more accurately.

I. INTRODUCTION

In ferromagnetic materials, magnetization (M) is not linearly proportional to the externally applied magnetic field strength (H), but depends on the past magnetization history of the material, a phenomenon called magnetic hysteresis. Considering its prevalence in the operation of most electrical engineering devices, such as transformers, motors, power electronics and magnetic recording devices, there is much commercial and research interest to measure and study hysteresis in magnetic materials. One technique uses a sophisticated piece of instrument called the vibrating-sample magnetometer^[1] (VSM) to measure induced voltage resulting from a vibrating magnetized sample.

In this paper, we constructed a low-cost alternative based on the TL071 op-amp integrator^[2], where our proxy for magnetization is the magnetic flux density (B) generated when an external magnetic field is applied on a ferromagnetic bulk sample.

We begin by laying out our experimental methods and the underlying theory (Section II), followed by results and data analysis (Section III), discussions (Section IV) and concluding remarks (Section V).

II. METHODS & THEORY

A. Measuring B-H curves using two solenoid coils

Our experimental setup consists of positioning the sample within a coaxial primary and secondary coil, which are assumed to behave like ideal solenoids experiencing the same magnetic flux attributed to the sample and a background flux that may arise from the sample holder consisting of a plastic sheath and copper cylinder. The primary coil is connected to a ca. 50 Hz AC voltage generator and the secondary coil to the input of an integrator circuit.

The external magnetic field applied on the sample is generated by passing an alternating current (AC) through the primary coil, the strength of which is obtained by measuring voltage V_x across a resistor R_p connected in series (**Figure 1**) and using the following relation (see **Table 1** for parameters and symbols):

$$H = I_p \frac{n_p}{L_p} = \frac{V_x}{R_p} \frac{n_p}{L_p} \quad (1)$$

^aCavendish Laboratory, University of Cambridge, JJ Thomson Ave, Cambridge CB3 0HE. E-mail: tkl35@cam.ac.uk

[†]Electronic Supplementary Information (ESI) available in the form of source code for data analysis: <https://github.com/KingLam26/hysteresis>

* Overleaf word count

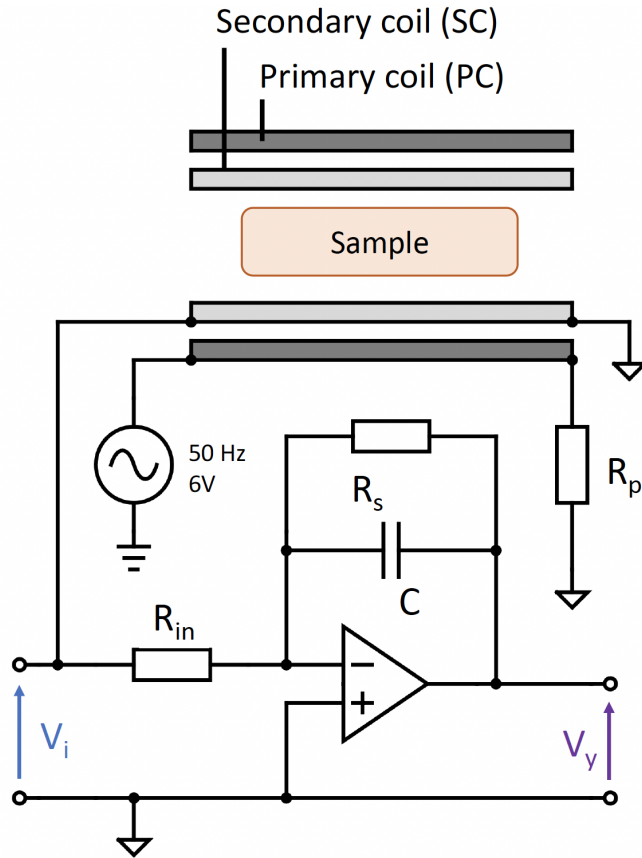


Figure 1 Experimental setup consisting of integrator circuit, primary and secondary coils. Voltages V_i , V_y and V_x are monitored using the PicoScope (2000 series) at various stages of the experiment.

Since V_x is time-varying, by Faraday's law of induction, an induced voltage ε_s will be generated in the secondary coil,

$$\varepsilon_s = -\frac{\partial \Phi}{\partial t} = \frac{n_s}{A_s} \frac{\partial \Phi}{\partial B} \quad (2)$$

Instead of measuring ε_s directly, we constructed an integrator circuit with ε_s fed into its input. The magnetic flux density is then recovered from

$$V_y = -\frac{1}{R_s C} \int \varepsilon_s dt = \frac{n_s A_s}{R_s C} B \quad (3)$$

The integrator circuit was designed to have low gain (G) feedback to avoid clipping in the op-amp output. A shunt resistor, $R_s \approx 1 \text{ M}\Omega$, was added to ensure any DC signal offsets, such as the input bias current of the TL071 op-amp used, do not cause the

Table 1 Circuit parameters and sample dimensions in SI units; effective sample lengths dictated by L_p , which is shorter than the actual sample lengths

Circuit parameters	Value
Integrator capacitance / C	$(473.6 \pm 0.2) \times 10^{-9}$
Integrator shunt resistance / R_s	$(9.855 \pm 0.005) \times 10^5$
Integrator input resistance / R_{in}	$(9.949 \pm 0.006) \times 10^3$
Primary coil resistance / R_p	2.1 ± 0.1
Primary coil turns / n_p	400
Secondary coil turns / n_s	500
Primary coil length / L_p	$(4.2 \pm 0.1) \times 10^{-2}$
Secondary coil diameter / D_s	$(5.1 \pm 0.1) \times 10^{-3}$
Sample dimensions	Value
Mild steel diameter / d_s	$(3.15 \pm 0.01) \times 10^{-3}$
Cu/Ni alloy diameter / d_s	$(4.99 \pm 0.01) \times 10^{-3}$
Transformer iron thickness / t	$(6.1 \pm 0.1) \times 10^{-4}$
Transformer iron width / w	$(4.22 \pm 0.01) \times 10^{-3}$
Sample cross-sectional area / A_s	$A_s = (\pi/4) d_s^2$

integrator output to drift and saturate.

In our final circuit design, theoretical gain is calculated as

$$G = \left| \frac{Z_C}{R_{in}} \right| = \left| \frac{i}{R_{in} \omega C} \right| = 0.6756 \pm 0.0005 \quad (4)$$

B. Experiment

First, we performed an initial system check to ensure the integrator is performing nominally at the planned operational frequency of around 50 Hz. This is achieved by using sinusoidal and square voltage functions produced from the TG315 function generator as input to the integrator.

Subsequently, we performed an air-core test (no sample) to estimate the “effective” magnetic permeability associated with the sample holder, which we expect to be close to but not necessarily equal to $\mu_r = 1$. We then performed hysteresis measurements on all three samples at room temperature (22°C), before attempting to broadly constrain the Curie temperature of the Cu/Ni alloy sample by repeating its measurement at 5°C, achieved by immersing the coils in an ice-water bath.

C. Data processing

Voltage measurements were recorded using the Pico-Scope program and exported as raw CSV data files. A python code repository was developed for data retrieval, analysis and plotting.

First, we spliced the multiple hysteresis loops obtained over several periods into individual loops. By treating each loop as an extensive polygon, we calculated its area to estimate power dissipation of each ferromagnetic sample per unit volume. Two separate techniques, shoelace algorithm (with CCW sort) and Python package Shapely^[3], were used for comparison and cross-checking. The multiple loops provided a first estimate on loop area error.

Next, we performed Monte Carlo error propagation, where the error associated with each (H, B) data point on the hysteresis curve was first calculated. We then artificially generated $N = 10^5$ different loops by randomly selecting (H, B) values at each point based on a Gaussian distribution for the error. The mean and standard deviation of the loop area were calculated as a function of increasing N to characterize their rate of convergence. Computation was performed on a Linux workstation (Intel Core i7-5820K Processor, 6-core, 3.30 GHz) and took around 10 hours. Moreover, a simple sensitivity analysis was performed to identify the greatest source of error among the independent variables.

Finally, we note that reasonable estimates of μ_r based on the initial magnetization curve require annealing the samples to above their Curie temperatures, where their magnetic spins become randomly aligned until a magnetic field is applied. As this was not performed in this experiment, we could only resort to a crude estimation of μ_r by approximating the initial magnetization curve by the positive ascent phase (as defined in **Figure 2**), and using

$$\mu_r = \frac{\partial B}{\partial H} \quad (5)$$

D. Fitting experimental data to the Jiles–Atherton model

Mathematical models of hysteresis are also useful in many theoretical and design problems. In this experiment, the ability to theoretically reconstruct the initial magnetization curve based on experimental data restricted to the hysteresis loop would be particularly invaluable in providing a better estimate of μ_r , compared to using the positive ascent phase.

The Jiles-Atherton (JA) model^[4] is widely used for describing the magnetization of soft magnetic materials due to its relative simplicity and intuitive physical meaning for its parameters. The premise of the model and governing equations our code is based on are elucidated in literature^[5].

Our optimization algorithm seeks to find input parameter values for the JA model that best fits our experimental data for a single hysteresis loop obtained for transformer iron at room temperature. Since it is useful to consider magnetization, which can be calculated from first principles, we first converted B, the parameter we measured, to M via

$$B = \mu H = \mu_0 (H + M) \quad (6)$$

where μ is the material permeability, and μ_0 is the permeability of free space.

We then defined a real valued objective function that computes the sum of squared errors (SSE) between experimental and modelled hysteresis curves, which we then minimized using the Python package Scipy^[7]. To evaluate how well our data fitted the JA model, we plotted the residues of the two (upper and lower) branches in the hysteresis curve and performed a χ^2 test, defined as follows

$$\chi^2 = \sum_i \left[\frac{y_i - E_i}{\sigma_i} \right]^2 \quad (7)$$

with y_i being the experimental data point (magnetization), E_i being the value predicted by the JA model

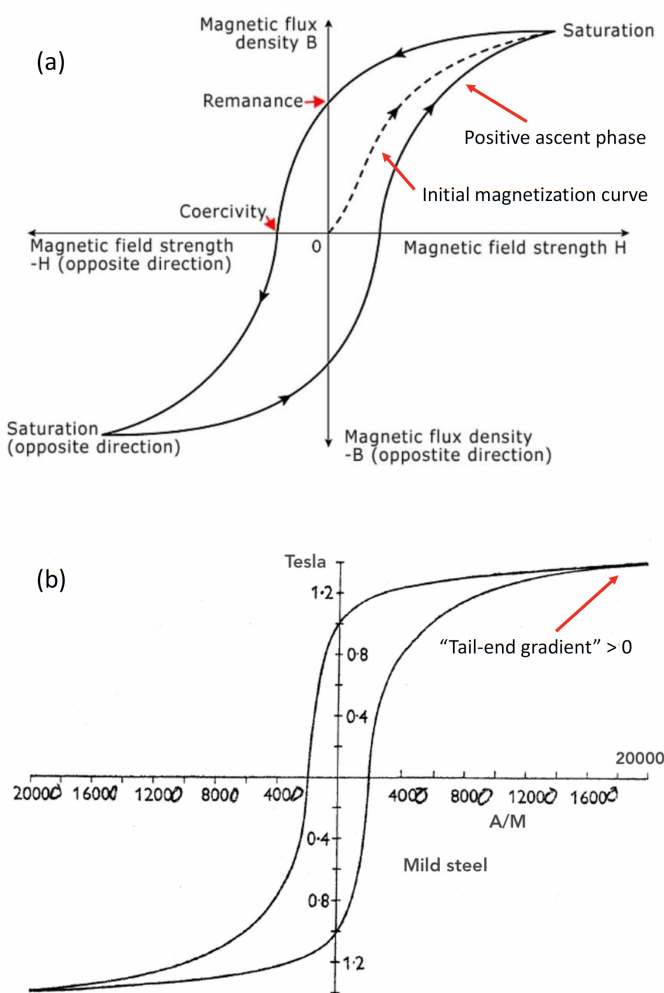


Figure 2 (a) The JA model accounts for all the important features in a typical hysteresis curve. Notably, it predicts that the curve should plateau to zero gradient near both ends of saturation. Figure reproduced and modified from literature^[5]. (b) In practice, a non-zero gradient linear B-H relation is often observed near saturation. Figure reproduced and modified from literature^[6].

using the same H value (obtained from experimental data), and $\sigma_i = \sqrt{E_i}$ in accordance with a Poisson distribution.

Finally, the non-zero “tail-end gradient” often observed in experimental data suggests the presence of “background” μ_r (**Figure 2**). Another plausible explanation lies in additional magnetization when the magnetic domains in the poly-crystalline sample orig-

inally aligned along the easy axis undergo dipole rotation to become aligned with the external field direction as the latter is increased further.

Since this phenomenon is not predicted by the JA model, our algorithm removes this discrepancy by subtracting this “tail-end gradient”, estimated by performing linear regression in that region, from the rest of the curve.

III. RESULTS & DATA ANALYSIS

A. Integrator circuit system check

We confirmed the integrator circuit is functioning nominally, as the output signals are the expected integrals of the input signals (**Figure 3**).

However, the experimentally determined gain was found to deviate from that calculated theoretically, at least within the error margins obtained, which is very likely a severe underestimation, considering the inability of the Picoscope to capture voltage errors arising from the integrator circuit.

$$V_{i,p-p} = 2.072 \pm 0.006$$

$$V_{y,p-p} = 1.560 \pm 0.012$$

$$G_{exp} = 0.753 \pm 0.006 \quad (8)$$

In particular, self and mutual inductances of the coils were assumed to be negligible, but may actually generate significant feedback to the circuit, presenting errors in the form of offsets and thereby increasing the overall random error of the voltage measurements.

B. Air-core test

Background magnetic permeability was determined by performing linear regression on the plot of V_y against V_x (**Figure 4**) and using Equations (1) and (3). The large $R^2 = 0.997$ value suggests a linear B-H relation fits the experimental data well, and μ_r

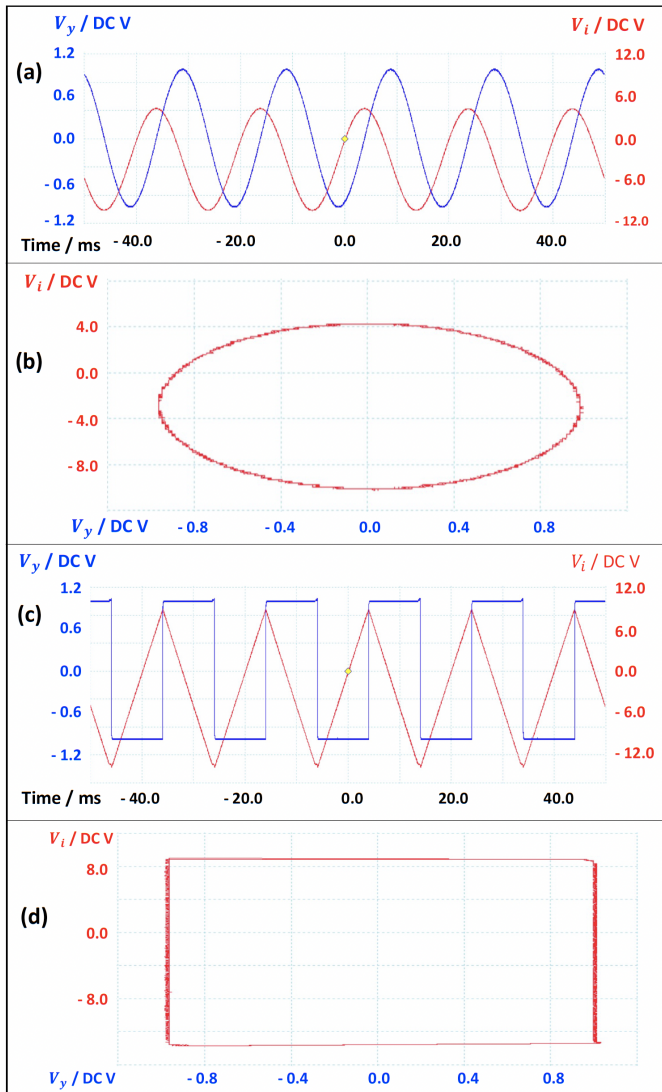


Figure 3 (a-b) Sinusoidal input with $f = 50.19 \pm 0.01$ Hz; elliptical Lissajous figure indicates sinusoidal output is $\pi/2$ phase-shifted. **(c-d)** Square wave input with same f gave in-phase triangular waveform as output, with a corresponding rectangular Lissajous figure.

is independent of H .

$$\frac{V_y}{V_x} = \frac{n_s A_s}{R_{in} C} \frac{n_p}{L_p R_p} \mu_r \mu_0 = (1.66 \pm 0.09) \times 10^{-2}$$

$$\mu_r = 1.34 \pm 0.01$$

$$(9)$$

As usual, voltage errors obtained from the PicoScope were most likely an underestimate. Nevertheless, μ_r is still significantly larger than 1, which might reflect the paramagnetic properties of the sample holder, and precision errors and noise in the inte-

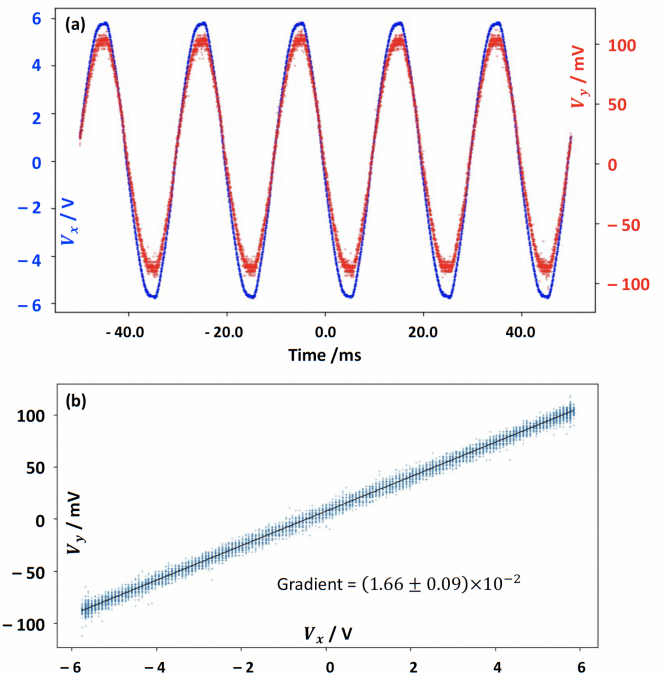


Figure 4 (a) Sinusoidal in-phase waveforms for both V_x and V_y with $f = 50.19 \pm 0.01$ Hz for the air core test. **(b)** Lissajous figure shows linear relation between the voltages.

grator circuit.

C. Hysteresis loops

The characteristic hysteresis loops (Figure 5) obtained for the three samples resembled those obtained in previous experiments^[6], displaying the key features of the hysteresis curve (Figure 2), including saturation of magnetization M_{sat} , coercivity and remanence (Table 2). Our results indicate all three samples are indeed ferromagnetic at room temperature, and that the system constructed is capable of quantitatively characterizing ferromagnetic properties of a material.

D. Power dissipation

In calculating the B-H loop area, we elected to use the polygon algorithm in the Shapely package as the shoelace algorithm we developed had a tendency to overestimate the tail end regions. Experimental data collected over 10 periods (200 ms), corresponding to

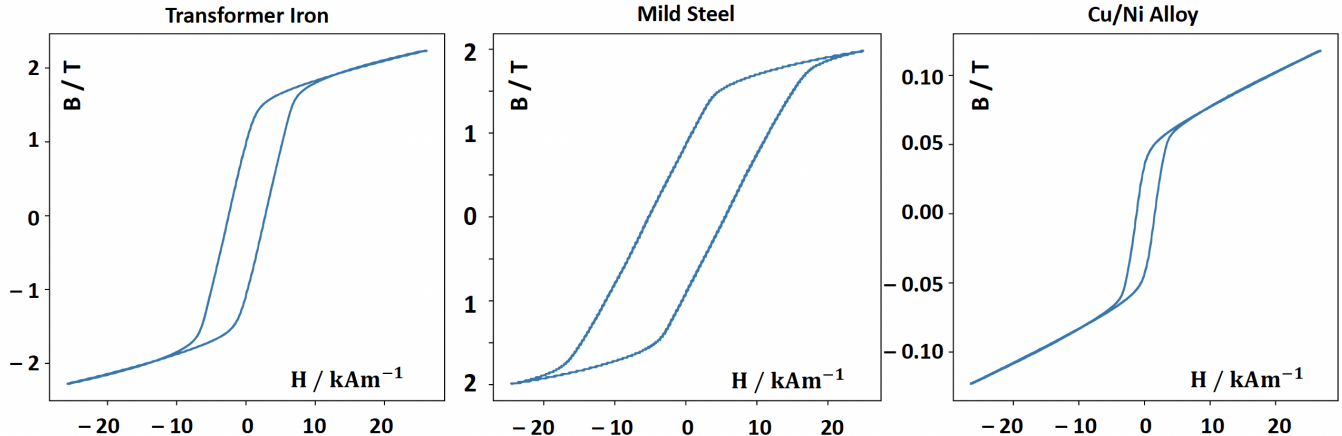


Figure 5 Ten consecutive hysteresis loops over a total time period of 200 ms for all three samples at room temperature, with mild steel displaying the highest remanence, magnetization at saturation (M_{sat}) and power dissipation per period. As expected, a non-zero “tail-end” gradient is observed at both ends of M_{sat} for all samples.

10 separate stable hysteresis loops showed very little variation in the (H , B) data, resulting in a very low standard deviation in the loop area (percentage error ca. 1%). In contrast, extracting a single loop and performing Monte Carlo error propagation (MCEP), taking into consideration sample dimension and circuit parameter errors, resulted in a more realistic error ΔA , that is easily two orders of magnitude larger (**Table 3**).

Considering the magnitude of ΔA in this particular experiment, $N = 2000$ artificial loops sufficed to constrain fluctuations in the mean and standard deviation of the loop areas to within 0.2%, thereby rendering further computation of more loops unnecessary.

The noticeably high ΔA for transformer iron can be traced to the measurement of sample width using a micrometer screw gauge, which is about an order of magnitude smaller than its length, and diameters of other samples, therefore resulting in an abnormally high percentage error. We confirmed this with a simple sensitivity analysis (**Table 4**), where we found that reducing the error in the thickness of the transformer iron sample by an order of magnitude gave loop area $A = 17300 \pm 1400$ (MCEP with $N = 2000$). Indeed, the easiest way to reduce error by around 5

Table 2 Approximate sample remanence and coercivity at room temperature derived from plots of the hysteresis loops, which generally agree with literature values^[6] to within an order of magnitude

Sample	Remanence / T	Coercivity / Am ⁻¹
Mild steel	0.8	5200
Trans. iron	1	2500
Cu/Ni alloy	0.03	1200

Table 3 Hysteresis loop areas and error estimates (SI units) obtained using standard deviation of 10 consecutive loops (*) versus Monte Carlo error propagation (†) for $N = 2000$ artificial loops constructed

Sample	Loop area*	Loop area†
Mild steel	37622 ± 30	38000 ± 4000
Transformer iron	17260 ± 20	17500 ± 7700
Cu/Ni alloy	201 ± 2	300 ± 100

times is to increase the thickness of the transformer iron sample to ca. 6 mm.

Next, we calculated magnetic power dissipation in the samples per unit volume (**Table 5**). Mild steel presents itself with the highest power loss while the Cu/Ni alloy dissipated less power than transformer iron. Considering minimal power loss is a highly desirable property when designing transformers, one might question the choice of transformer iron over the

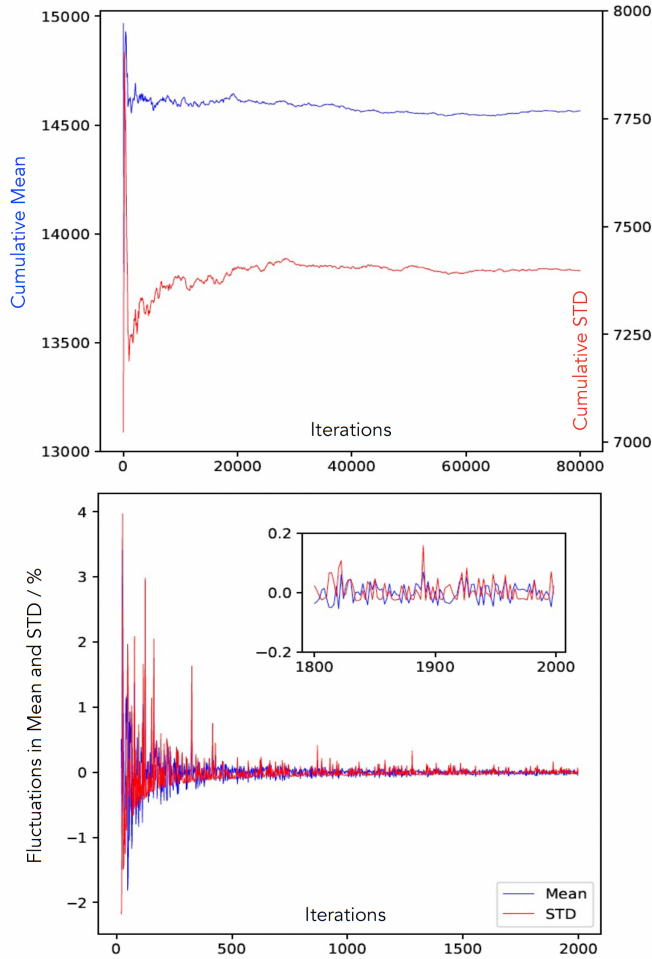


Figure 6 Monte Carlo error propagation with mean, standard deviation and corresponding fluctuations plotted against number of iterations.

Table 4 Sensitivity analysis for transformer iron performed by reducing error in dependent variables by an order of magnitude in turn, before performing MCEP with $N = 2000$ to estimate loop area and associated error (more significant figures included for demonstration)

Variable	Loop area	Error
None	17500	7700
R_p	17300	3500
L_p	17200	6800
C	17700	7700
R_s	17200	7400
t	17300	1400
w	17300	7500
All of the above	17200	80

Cu/Ni alloy. This question is put to rest when the low Curie temperature of the latter is subsequently

Table 5 Sample power loss and upper bound on relative permeability (μ_r)

Sample	Power loss / mW m^{-3}	μ_r
Mild steel	12.4 ± 1.3	$\lesssim 110$
Transformer iron	1.9 ± 0.8	$\lesssim 300$
Cu/Ni alloy	0.25 ± 0.08	$\lesssim 25$

Table 6 Parameters used for the JA model

Param. / Units	Initial guess / Bounds	Converged value
a / Am^{-1}	$1.9\text{e}3 / (1.6\text{e}3, 2.4\text{e}3)$	$2.38\text{e}3$
α	$1.9\text{e}-3 / (1\text{e}-12, 1\text{e}-1)$	$2.69\text{e}-3$
c	$5.8\text{e}-12 / (0, 1)$	$3.28\text{e}-8$
k / Am^{-1}	$3.1\text{e}3 / (0, 4\text{e}3)$	$2.90\text{e}3$
M_{sat} / Am^{-1}	$1.6\text{e}6 / (1.5\text{e}6, 1.5\text{e}7)$	$1.62\text{e}6$

demonstrated.

Finally, we crudely estimated an upper bound on μ_r for the different samples at room temperature by subtracting any “background” μ_r attributed to the non-zero tail-end gradient from the positive ascent phase (**Table 5**).

E. Fitting the JA model for transformer iron

The inherent quantization of the voltages measured by the PicoScope prompted us to first remove adjacent (H, B) data points with the same H value, to avoid singularities when calculating the gradient of the hysteresis curve. Next, the gradient correction routine was performed to remove the effects of the tail-end gradient, which was estimated by considering data points beyond $H = \pm 20000 \text{ Am}^{-1}$. A series of optimization runs were then performed to identify an ideal H value above and below which to truncate the data points. The initial magnetization curve in our JA model is generated starting from the origin in steps of $H = 20 \text{ Am}^{-1}$.

Unequivocally, our experimental data fitted the JA model poorly, as suggested by the large χ^2 value compared to the number of data points, and the large residue “chunks” (**Figure 7**) in the residue plot drove

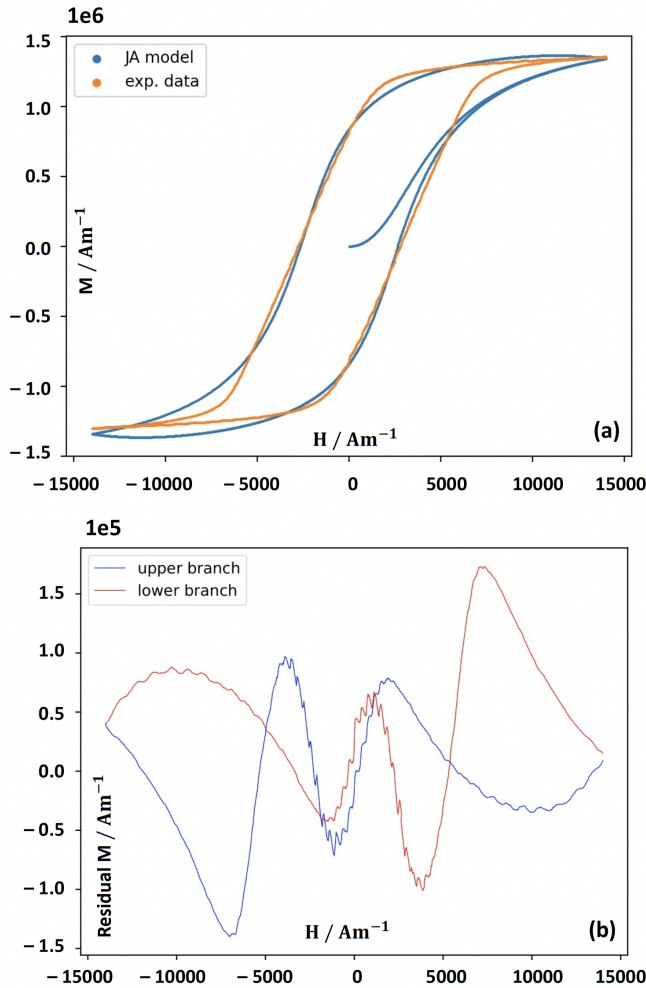


Figure 7 (a) Best fit of a single transformer iron hysteresis loop to the JA model with truncation beyond $H = \pm 14000$ Am^{-1} with a predicted initial magnetization curve from which a better estimate of μ_r could be obtained. (b) Residues of the JA model for the two branches in the hysteresis loop. $\chi^2 \approx 2.6 \times 10^7 \gg N = 3116$.

the nail in the coffin. Moreover, we also found the JA model to be extremely sensitive to the initial parameter guess. For example, varying the initial parameters by as little as 1% resulted in convergence to a separate set of parameters, and in other cases, failure to converge. This indicates that the SSE objective function exhibits many local minima, rendering gradient optimization techniques ineffective.

F. Estimating Curie temperature of the Cu/Ni alloy

At elevated temperatures (ca. 50°C), the magnetiza-

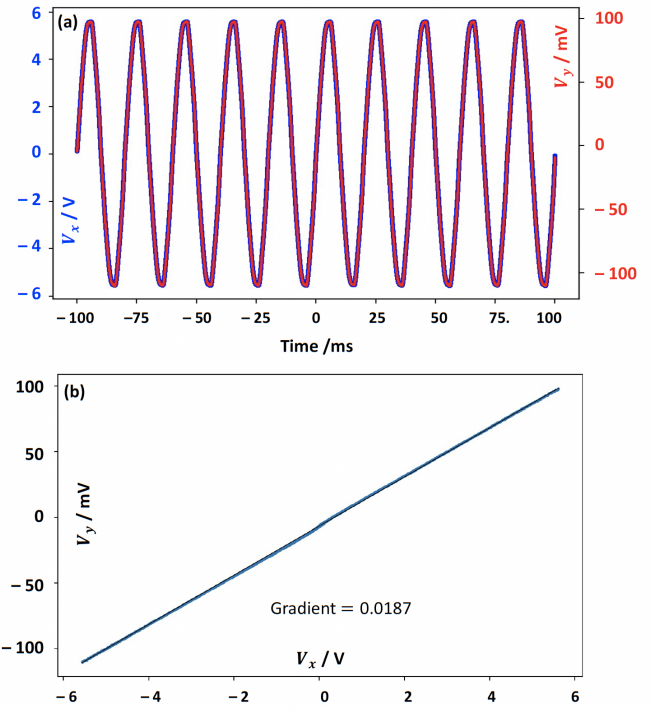


Figure 8 (a) Sinusoidal in-phase waveforms for both V_x and V_y with $f = 50.19 \pm 0.01$ Hz for the Cu/Ni alloy at ca. 50°C. (b) The hysteresis loop has collapsed to a positive proportional linear relation between V_x and V_y , with negligible loop area. The inability of the PicoScope to capture reasonable voltage errors prompted us to exclude error in the gradient calculated from linear regression.

tion of the Cu/Ni alloy no longer exhibits hysteresis, with negligible loop area and positive proportional relation between the B-field measured and the applied H-field. We constrained the Curie temperature of the Cu/Ni alloy to between room temperature and ca. 50°C, at which the material transitions from the ferromagnetic to paramagnetic regime. By performing linear regression on the plot of V_y against V_x (Figure 8), we estimated $\mu_r \approx 1.51$.

IV. DISCUSSION

A. Experimental errors

As demonstrated in the sensitivity analysis, sample dimensions are responsible for introducing the greatest source of error, which could simply be reduced by

fabricating samples with larger dimensions to reduce percentage error.

Moreover, the inability of the Picoscope to adequately quantify errors in the integrator circuit means that the hysteresis loops measured should be corroborated by other more sophisticated methods such as VSM or magneto-optic Kerr effect systems^[8], especially if the material being studied is to be used for research or commercial studies.

Heat generation due to magnetic power dissipation in the sample and Joule heating in the coils could be better mitigated through a combination of passive and active cooling systems, such as heat sinks and fans. For larger samples with greater heat dissipation, one might consider water cooling by designing the samples with internal channels to pass water through, so that any temperature changes can be damped by exploiting the higher heat capacity of water.

Crucially, we strongly recommend introducing the ability to measure real-time sample temperature using a thermocouple since magnetization is temperature dependent, as predicted by the classical Brillouin magnetization theory with positive-feedback mean-field modification^[9]. This dependence was shown to be of increasing significance when sample temperature approaches the Curie temperature, which was also observed in this experiment with the Cu/Ni alloy. Precise sample temperature control can also be achieved by introducing electric heaters and thermoelectric coolers, such as silicone heater mats and Peltier coolers respectively. These options are sufficiently small in size and can be incorporated in our existing experimental setup without much anticipated trouble.

B. Studying magnetic susceptibility above Curie temperature

The ability to track the evolution of the hysteresis loop as a function of sample temperature using a ther-

mocouple would not only allow us to better constrain the Curie temperature, but also open a new avenue to study other phenomena, such as the validity of the Curie–Weiss law which describes the magnetic susceptibility χ of a ferromagnet in the paramagnetic region above the Curie temperature, T_C .

$$\chi = \frac{C}{T - T_C} \quad (10)$$

where C is a material-specific Curie constant and T is the absolute temperature of the sample. The Cu/Ni alloy is unique in having a low and therefore easily accessible T_C which we can exploit to study the parameter space around T_C .

C. Search for a better theoretical model

Finally, while the JA model was ultimately a poor fit for our data, we have demonstrated conceptually the usefulness of fitting data to a theory that can predict the initial magnetization curve. This motivates the search for alternative models, such as the vectorial incremental nonconservative consistent hysteresis (VINCH) model^[10] and the Stoner–Wohlfarth model^[11]. In practice, the presence of other materials and components besides the sample and two coils means the electromagnetic field in our experimental setup is vastly more complicated, which may warrant the use of modern finite element analysis techniques, such as FEMM (Finite Element Method Magnetics) or the vector hysteresis model in COMSOL Multiphysics.

Concerning optimization techniques, in the context of the JA model, we found that the SSE objective function had many local minima, which rendered local optimisation techniques ineffective, even though they are easily implementable. More sophisticated global optimization techniques like simulated annealing methods^[12] and genetic algorithms^[13;14] have been proposed and should be employed if similar difficulties are encountered.

V. CONCLUSION

A system consisting of an integrator circuit and two solenoid coils was used to quantitatively characterize the magnetic properties of several ferromagnetic materials (mild steel, transformer iron, and Cu/Ni alloy). Its simplicity and low-cost architecture makes it particularly useful for pedagogical purposes, or preliminary comparisons between different materials. Initial system checks using sinusoidal and square input signals confirmed the integrator circuit was functioning nominally at ca. 50 Hz. Based on the characteristic hysteresis loops obtained for the three samples, key magnetic properties were determined, including remanence, coercivity, and power dissipation. Mild steel was the most ferromagnetic material, with power dissipation at $12.4 \pm 1.3 \text{ mW m}^{-3}$. Our system was also able to detect the ferromagnetic and paramagnetic regime change in the Cu/Ni alloy, paving the way for modifications towards accurate measurements of the Curie temperature. Finally, while our experimental data was found to fit the JA model poorly, we demonstrate this concept can be applied to other potentially better models that can predict the initial magnetization curve, which will provide a better way to estimate the magnetic permeability of the material more accurately.

ACKNOWLEDGEMENTS

This material is based upon work supported by Cavendish Laboratory Teaching Labs, University of Cambridge, as part of the NST Physics Part IB course.

REFERENCES

- [1] Yakovlev N. L., Chen H., and Zhang K. Two-axis magnetisation analysis of epitaxial cobalt films. *Journal of Nanoscience and Nanotechnology*, **11**(3):2575–2578, 2011.
- [2] Texas Instruments. Tl07xx low-noise fet-input operational amplifiers. URL <https://www.ti.com/product/TL071>.
- [3] Gillies S. (2007). Shapely: manipulation and analysis of geometric objects. URL <https://github.com/Toblerity/Shapely>.
- [4] Jiles D.C. and Atherton D.L. Theory of ferromagnetic hysteresis. *Journal of Magnetism and Magnetic Materials*, **61**:48–60, 1986.
- [5] Khemani V., Azarian M. H., and Pecht M. G. Efficient identification of jiles–atherton model parameters using space-filling designs and genetic algorithms. *Eng*, **3**(3):364–272, 2022.
- [6] University of Cambridge Department of Physics. Measurement and Experimental Physics. *NST IB Physics A and B Practicals Class Manual*, (6):50–53, 2022.
- [7] Pauli Virtanen, Ralf Gommers, Travis E. Oliphant, Matt Haberland, Tyler Reddy, Cournapeau ..., and SciPy 1.0 Contributors. SciPy 1.0: Fundamental Algorithms for Scientific Computing in Python. *Nature Methods*, **17**:261–272, 2020. doi: 10.1038/s41592-019-0686-2.
- [8] Allwood D. A., Xiong G., Cooke M. D., and Cowburn R. P. Magneto-optical kerr effect analysis of magnetic nanostructures. *Journal of Physics D: Applied Physics*, **36**(18):2175, 2003.
- [9] Harrison R. G. Calculating the spontaneous magnetization and defining the curie temperature using a positive-feedback model. *Journal of Applied Physics*, **115**:3, 2014.
- [10] François-Lavet V., Henrotte F., Stainier L., Noels L., and Geuzaine C. Vectorial incremental nonconservative consistent hysteresis model. *5th International Conference on Advanced COmputational Methods in Engineering*, 2011.
- [11] Mathews S. A., Ehrlich A. C., and Charipar N. A. Hysteresis branch crossing and the

- stoner–wolfarth model. *Scientific reports*, **10** (1):1–7, 2020.
- [12] Bai B., Wang J., and Zhu K. Identification of the Jiles - Atherton model parameters using simulated annealing method. *Proceedings of the IEEE Electrical Machines and Systems (ICEMS)*, 2011.
- [13] Chwastek K. and Szczygłowski J. Identification of a hysteresis model parameters with genetic algorithms. *Mathematics and Computers in Simulation*, **71**:206–211, 2006.
- [14] Wilson P., Ross J., and Brown A. Optimizing the jiles-atherton model of hysteresis by a genetic algorithm. *IEEE Transactions on Magnetics*, **37**:989–993, 2001.